

# Molecular basis of the high-affinity activation of type 1 ryanodine receptors by imperatoxin A

Chul Won LEE\*, Eun Hui LEE\*, Koh TAKEUCHI†, Hideo TAKAHASHI†, Ichio SHIMADA†, Kazuki SATO‡, Song Yub SHIN§, Do Han KIM\* and Jae Il KIM\*<sup>1</sup>

\*Department of Life Science, Kwangju Institute of Science and Technology, Kwangju 500-712, South Korea, †Graduate School of Pharmaceutical Sciences, The University of Tokyo, Tokyo 113-0033, Japan, ‡Department of Environmental Science, Fukuoka Women's University, Fukuoka 813-8529, Japan, and §Research Center for Proteinaceous Materials, Chosun University, Kwangju 501-759, South Korea

Both imperatoxin A (IpTx<sub>a</sub>), a 33-residue peptide toxin from scorpion venom, and peptide A, derived from the II–III loop of dihydropyridine receptor (DHPR), interact specifically with the skeletal ryanodine receptor (RyR1), which is a Ca<sup>2+</sup>-release channel in the sarcoplasmic reticulum, but with considerably different affinities. IpTx<sub>a</sub> activates RyR1 with nanomolar affinity, whereas peptide A activates RyR1 at micromolar concentrations. To investigate the molecular basis for high-affinity activation of RyR1 by IpTx<sub>a</sub>, we have determined the NMR solution structure of IpTx<sub>a</sub>, and identified its functional surface by using alanine-scanning analogues. A detailed comparison of the functional surface profiles for two peptide activators revealed that IpTx<sub>a</sub> exhibits a large functional surface area (approx. 1900 Å<sup>2</sup>, where 1 Å = 0.1 nm), based on a short double-stranded antiparallel β-sheet structure, while peptide A bears a much smaller functional

surface area (approx. 800 Å<sup>2</sup>), with the five consecutive basic residues (Arg<sup>681</sup>, Lys<sup>682</sup>, Arg<sup>683</sup>, Arg<sup>684</sup> and Lys<sup>685</sup>) being clustered at the C-terminal end of the α-helix. The functional surface of IpTx<sub>a</sub> is composed of six essential residues (Leu<sup>7</sup>, Lys<sup>22</sup>, Arg<sup>23</sup>, Arg<sup>24</sup>, Arg<sup>31</sup> and Arg<sup>33</sup>) and several other important residues (His<sup>6</sup>, Lys<sup>8</sup>, Arg<sup>9</sup>, Lys<sup>11</sup>, Lys<sup>19</sup>, Lys<sup>20</sup>, Gly<sup>25</sup>, Thr<sup>26</sup>, Asn<sup>27</sup> and Lys<sup>30</sup>), indicating that amino acid residues involved in RyR1 activation make up over the half of the toxin molecule with the exception of cysteine residues. Taken together, these results suggest that the site where peptide A binds to RyR1 belongs to a subset of macrosites capable of being occupied by IpTx<sub>a</sub>, resulting in differing the affinity and the mode of activation.

**Key words:** excitation–contraction coupling, imperatoxin A, NMR, peptide A, ryanodine receptor, solution structure.

## INTRODUCTION

In cardiac and skeletal muscle, the ryanodine receptor (RyR) is a Ca<sup>2+</sup>-release channel in the sarcoplasmic reticulum (SR) and the dihydropyridine receptor (DHPR) is a voltage-gated L-type Ca<sup>2+</sup> channel. These two receptors play central roles in the sarcolemma excitation–contraction (E–C) coupling that links an electrical stimulus (depolarization) to release of Ca<sup>2+</sup> from the SR [1]. Cardiac and skeletal muscles express different subtypes of DHPRs and RyRs, causing tissue-specific E–C coupling. In cardiac muscle, E–C coupling is induced by the entry of extracellular Ca<sup>2+</sup> through DHPR, whereas skeletal type E–C coupling requires a direct physical coupling between DHPR and RyR [2,3]. Evidence supporting this physical coupling between skeletal DHPR and RyR1 (skeletal type RyR) includes successful co-immunoprecipitation [4] and identification of regions involved in the physical coupling between the two channels. Specifically, interactions have been observed between portions of the α<sub>1</sub> subunit of DHPR, including the II–III loop, the III–IV loop and the C-terminal segment, and the Arg<sup>1076</sup>–Asp<sup>1112</sup> region of RyR1 [5–12]. It has been proposed that these interactions cause orthograde signalling from DHPR to RyR1 for activation of RyR1, and retrograde signalling from RyR1 to DHPR for RyR1-mediated enhancement of Ca<sup>2+</sup> current [11,13].

Imperatoxin A (IpTx<sub>a</sub>), a 33-amino-acid peptide from the venom of the scorpion, *Pandinus imperator*, was the first peptide

toxin found to activate RyR1 with high potency and affinity, and it has been used in several biochemical and biophysical studies related to the E–C coupling [14,15]. Interestingly, it has been suggested that IpTx<sub>a</sub> activates RyR1 by mimicking a domain of DHPR that is critical for triggering Ca<sup>2+</sup> release. Using synthetic peptides corresponding to small segments of the II–III loop in skeletal DHPR, El-Hayek et al. [7] found that only the N-terminal portion (peptide A; Thr<sup>671</sup>–Leu<sup>690</sup>) was capable of activating RyR1, and subsequently identified a ten-residue active region (Arg<sup>681</sup>–Leu<sup>690</sup>) [16]. In addition, Gurrola et al. [17] reported that a peptide A-containing segment (Glu<sup>666</sup>–Leu<sup>690</sup>) might bind to the same RyR1 site as IpTx<sub>a</sub>, as shown by the results of competitive binding of <sup>125</sup>I-labelled IpTx<sub>a</sub> to the SR. This was additionally supported by the report that both peptides produced almost identical changes, with non-additive effects, in RyR1 gating characteristics [18]. Although these observations strongly suggested that IpTx<sub>a</sub> and peptide A share a common binding site on RyR1, the two peptide activators show very low sequence identity (approx. 18%), very different molecular structures, and considerably different affinities in RyR1 activation. IpTx<sub>a</sub> activates RyR1 with nanomolar affinity, whereas peptide A activates RyR1 at micromolar concentrations [17].

In order to examine the molecular basis by which two peptide activators, IpTx<sub>a</sub> and peptide A, act at a common site on RyR1 with different affinities, the present study reports the solution structure of IpTx<sub>a</sub> as determined by NMR spectroscopy and

Abbreviations used: ω-CTX, ω-conotoxin; DHPR, dihydropyridine receptor; DQF-COSY, double-quantum-filtered COSY; E–C, excitation–contraction; Fmoc, 9-fluorenylmethoxycarbonyl; HOHAHA, homonuclear Hartmann–Hahn; IpTx<sub>a</sub>, imperatoxin A; wIpTx<sub>a</sub>, wild-type IpTx<sub>a</sub>; NOE, nuclear Overhauser effect; PEG, poly(ethylene glycol); RyR, ryanodine receptor; RMSD, root mean square difference; RyR1, skeletal RyR; SR, sarcoplasmic reticulum.

<sup>1</sup> To whom correspondence should be addressed (e-mail jikim@kjst.ac.kr).

The co-ordinates of IpTx<sub>a</sub> have been deposited in the RCSB (Research Collaboratory for Structural Bioinformatics) Protein Data Bank under the accession code 1IE6.

dynamic simulated annealing calculations, and we have combined this structural information with the results of [ $^3\text{H}$ ]ryanodine binding assays using alanine-scanning analogues. On the basis of the structure–activity relationships for IpTx<sub>a</sub>, we propose that the peptide A-binding site on RyR1 belongs to a subset of macro-sites capable of being occupied by IpTx<sub>a</sub>, resulting in the observed differences in RyR1 affinity and activation. Furthermore, a comparative structural analysis with the cone-snail  $\omega$ -conotoxin MVIIC ( $\omega$ -CTX-MVIIC), a neuronal P/Q-type calcium-channel blocker, revealed that the characteristic shape of charged surface rather than globular shape is important to the interaction with RyR1, thus providing a structural insight for the specific interaction mode of RyR1-targeting peptide effectors.

## MATERIALS AND METHODS

### Materials

Fmoc (9-fluorenylmethoxycarbonyl) amino acids and other reagents used for peptide synthesis were obtained from Applied Biosystems. Fmoc-preloaded resin was obtained from Watanabe Chemical Industries (Hiroshima, Japan). [ $^3\text{H}$ ]ryanodine was obtained from NEN Life Science Products (Torrance, CA, U.S.A.). All other reagents were of high-purity reagent grade from Sigma Chemical Co.

### Peptide synthesis of wild-type IpTx<sub>a</sub> (wIpTx<sub>a</sub>) and analogues

Peptide synthesis was conducted on an Applied Biosystems model 433A peptide synthesizer. The linear precursors of wIpTx<sub>a</sub> and alanine-scanning analogues were synthesized by solid-phase Fmoc chemistry starting from Fmoc-Arg(2,2,5,7,8-pentamethylchroman-6-sulphonyl)-Alko or Fmoc-Ala-Alko resin and using a variety of blocking groups for amino acid protection. After cleavage by trifluoroacetic acid, crude linear peptides were extracted with 2 M ethanoic acid, diluted to final peptide concentrations of 25  $\mu\text{M}$  in a solution of 1 M ammonium acetate and 2.5 mM reduced/0.25 mM oxidized glutathione adjusted to pH 7.8 with aqueous  $\text{NH}_4\text{OH}$ , and stirred slowly at 4 °C for 2–3 days. The folding reactions were monitored by HPLC. The crude oxidized products were purified by successive chromatography with CM-cellulose CM-52 and preparative HPLC with  $\text{C}_{18}$  silica columns. The purity of all analogues was confirmed by analytical HPLC and MALDI-TOF-MS (matrix-assisted laser-desorption ionization–time-of-flight MS) measurements.

### CD measurements of wIpTx<sub>a</sub> and analogues

CD spectra were measured on a JASCO J-750 spectropolarimeter in solution (0.01 M sodium phosphate in water, pH 7.0) at 20 °C with a quartz cell of path length 1 mm. The spectra were expressed as molecular ellipticity [ $\theta$ ] in  $\text{deg} \cdot \text{cm}^2 \cdot \text{dmol}^{-1}$ .

### NMR measurements of wIpTx<sub>a</sub>

NMR spectra were recorded on a Bruker DRX 600 spectrometer. All two-dimensional NMR experiments [i.e. DQF-COSY (double-quantum-filtered COSY) [19], E-COSY (exclusive COSY) [20], HOHAHA (homonuclear Hartmann–Hahn) [21] and NOESY [22]] were performed with standard pulse sequences and phase cycling. HOHAHA spectra were recorded with mixing times of 60 and 80 ms. NOESY spectra were recorded with mixing times of 100, 200 and 300 ms. In all experiments, 512 increments of 2048 data points were recorded with 64–128 trans-

ients and were zero-filled once along the  $t_1$  dimension. A complete set of the two-dimensional spectra was recorded at 27 °C (pH 3.4). Synthesized wIpTx<sub>a</sub> (a final concentration of 5 mM) was dissolved in 0.2 ml of water containing  $^2\text{H}_2\text{O}$  at 10% (v/v) or 99.9% (v/v). Spectra were processed and analysed with Bruker XWIN-NMR software.

### Structure calculations of wIpTx<sub>a</sub>

Observed NOE (nuclear Overhauser effect) data were classified into four distance ranges, 1.8–2.7, 1.8–3.5, 1.8–5.0 and 1.8–6.0 Å (1 Å = 0.1 nm), corresponding to strong, medium, weak and very weak NOE values respectively. Pseudo-atoms were used for the methyl protons or the non-stereospecifically assigned methylene protons [23]. Correcting factors for the use of pseudo-atoms were added to the distance constraints. In addition, 0.5 Å was added to the distance constraints involving methyl protons [24]. For each disulphide bond, three distance constraints,  $S(i)-S(j)$ ,  $S(i)-C^\beta(j)$  and  $S(j)-C^\beta(i)$ , were used with target values set to 2.02 ( $\pm 0.02$ ), 2.99 ( $\pm 0.5$ ) and 2.99 ( $\pm 0.5$ ) Å respectively [25].

All calculations were performed using the X-PLOR 3.1 program [26] running on a SGI O2 workstation. Three-dimensional structures were calculated on the basis of distance and torsion angle constraints experimentally derived with dynamic simulated annealing protocols. The 20 best structures were chosen for structural analysis, based on the X-PLOR energy and best fit. The structures were analysed with the PROCHECK-NMR [27] and PROMITIF [28] software packages. Structural figures were generated with the MOLMOL program [29] and the INSIGHT II 2000 program (Accelrys Inc.).

### Isolation of SR vesicles

A heavy fraction of SR was prepared from rabbit back and leg fast twitch muscles with a modification of the previously described method [30]. Briefly, about 150 g of muscle was homogenized in a Waring blender with 4 vol. of 2.5 mM NaOH for six bursts of 20 s at intervals of 3 min. During the homogenization, the pH was adjusted to 6.8 with NaOH. The suspension was centrifuged at 10 000  $g$  for 3 min in a No. 9 rotor in a Hanil Supra22K centrifuge. The supernatant was filtered through eight layers of cheesecloth and then through Whatman filter paper (No. 4). After re-adjusting the pH to 6.8, if necessary, the filtrate was centrifuged again at 17 000  $g$  for 30 min in the above apparatus. The pellets were resuspended in the final buffer consisting of 0.15 M KCl, 20 mM Mops (pH 6.8) and 0.3 M sucrose in the presence of the following protease inhibitors: pepstatin (1  $\mu\text{M}$ ), leupeptin (1  $\mu\text{M}$ ), PMSF (100  $\mu\text{M}$ ) and trypsin inhibitor (1  $\mu\text{M}$ ). The suspension was centrifuged again at 17 000  $g$  for 30 min in a No. 7 rotor in a Hanil Supra22K centrifuge. The pellets were resuspended in the same final buffer and the final protein concentration was determined by the Bradford method [30a] using BSA as the standard. The obtained SR was quickly frozen in liquid  $\text{N}_2$  and then stored at  $-70$  °C until use.

### [ $^3\text{H}$ ]Ryanodine binding assay with wIpTx<sub>a</sub> and analogues

[ $^3\text{H}$ ]Ryanodine binding to rabbit skeletal SR vesicles was performed as previously described [31] with some modifications. Briefly, 0.04 mg of skeletal SR vesicles was incubated with various concentrations of wIpTx<sub>a</sub>, or one of the analogues, for 2 h at 37 °C in a reaction mixture of 250  $\mu\text{l}$  {0.2 M KCl, 20 mM Mops (pH 7.3), 5 nM [ $^3\text{H}$ ]ryanodine and 10  $\mu\text{M}$  free  $\text{Ca}^{2+}$ }. After incubation, 100  $\mu\text{l}$  of poly(ethylene glycol) (PEG) solution (30%

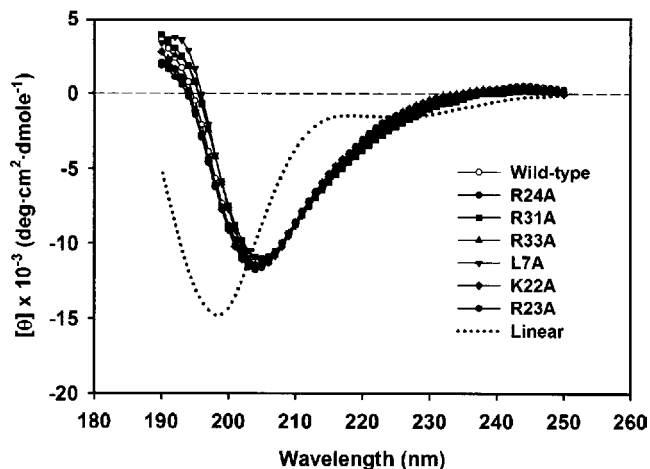


**Figure 1** CD spectra of *wIpTx<sub>a</sub>* and its analogues

The measurement was carried out in the UV range of 250–190 nm on a JASCO J-750 spectropolarimeter in solution (0.01 M sodium phosphate, pH 7.0) at 20 °C.

PEG, 1 mM EDTA and 50 mM Tris, pH 7.3) was added to each vial and was incubated for 5 min at room temperature (25 °C). Precipitated protein was sedimented for 5 min at 12 000 g using an Eppendorf microcentrifuge, and the pellets were rinsed twice with 0.6 ml of the relevant ryanodine-binding buffer without radioactive ryanodine. The pellets were then solubilized in 100  $\mu$ l of Soluene 350 (Packard) at 70 °C for 30 min, after which 4 ml of cocktail [Picofluor (Packard)] was added and the radioactivity was measured by liquid scintillation [32]. To minimize non-specific binding, 100-fold of non-radioactive ryanodine (Calbiochem) was included.

### Statistical analysis

Results are given as means  $\pm$  S.E.M. with the number of experiments. The S.E.M. is included within the Figure legends or indicated by error bars. Individual activation curves of RyR1 by *wIpTx<sub>a</sub>* and analogues were fitted with the Hill equation using the Origin 4.1 software package (RockWare, Golden, CO, U.S.A.).

## RESULTS AND DISCUSSION

### Synthesis of *wIpTx<sub>a</sub>* and analogues

Linear precursors of *wIpTx<sub>a</sub>* and its alanine-scanning analogues were assembled by solid-phase methodology. The crude linear precursors were air-oxidized, and the properly folded products were purified by ion-exchange chromatography and reverse-phase HPLC (1–4 % yield from the starting resin). CD spectra showed that secondary structures of all analogues, including L7A (Leu<sup>7</sup>  $\rightarrow$  Ala), K22A (Lys<sup>22</sup>  $\rightarrow$  Ala), R23A (Arg<sup>23</sup>  $\rightarrow$  Ala), R24A (Arg<sup>24</sup>  $\rightarrow$  Ala), R31A (Arg<sup>31</sup>  $\rightarrow$  Ala) and R33A (Arg<sup>33</sup>  $\rightarrow$  Ala), were similar to that of *wIpTx<sub>a</sub>* (Figure 1). Exceptionally, the linear analogue (Ala<sup>3,10,16,17,21,32</sup>)*IpTx<sub>a</sub>*, which simultaneously replaced all six cysteine residues with alanine residues, showed a random conformation with a large negative Cotton effect (around 198 nm), indicating that the three intramolecular disulphide bonds in *wIpTx<sub>a</sub>* play an important role in maintaining its overall structure.

### Structure calculations of *wIpTx<sub>a</sub>*

Complete proton assignments of all 33 amino acids in synthetic *wIpTx<sub>a</sub>* were determined using traditional two-dimensional NMR sequential assignment techniques [33]. Identification of the amino acid spin system was based on scalar coupling patterns observed in DQF-COSY and HOHAHA experiments, complemented with the results of NOESY measurements. Figure 2 shows the NH-C <sup>$\alpha$</sup> H

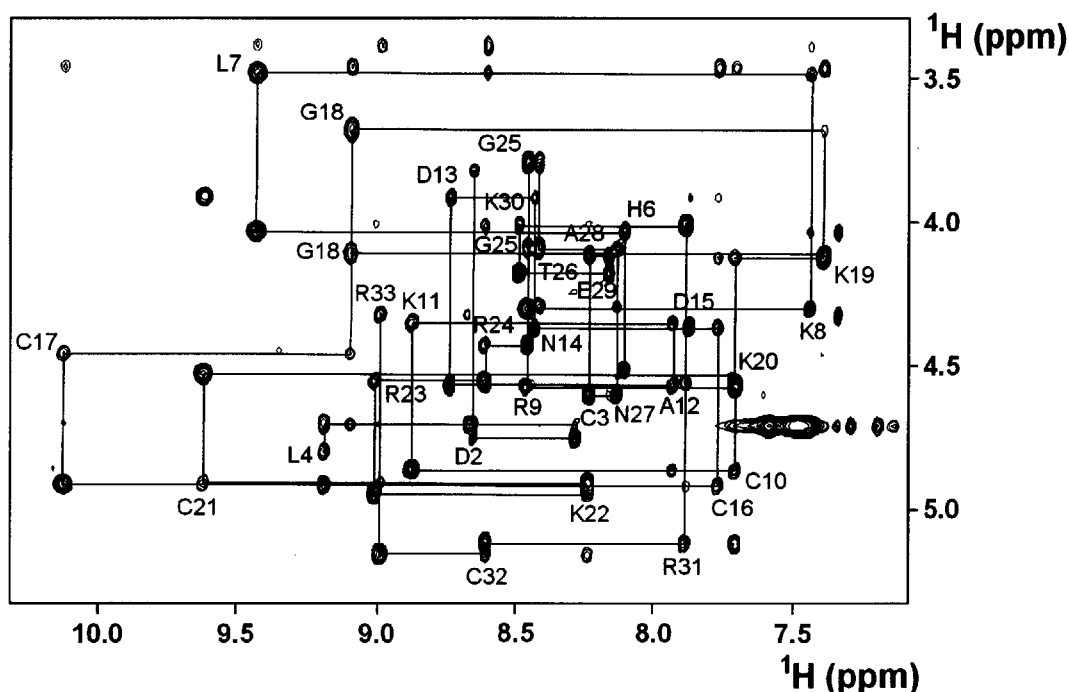


**Figure 2** Sequential  $d_{\alpha N}(i, i + 1)$  NOE connectivity for residues 2–33 in the NOESY spectrum observed with a mixing time of 300 ms

Intra-residue NH-C <sup>$\alpha$</sup> H cross-peaks are labelled with the residue numbers by standard single-letter amino acid abbreviations.

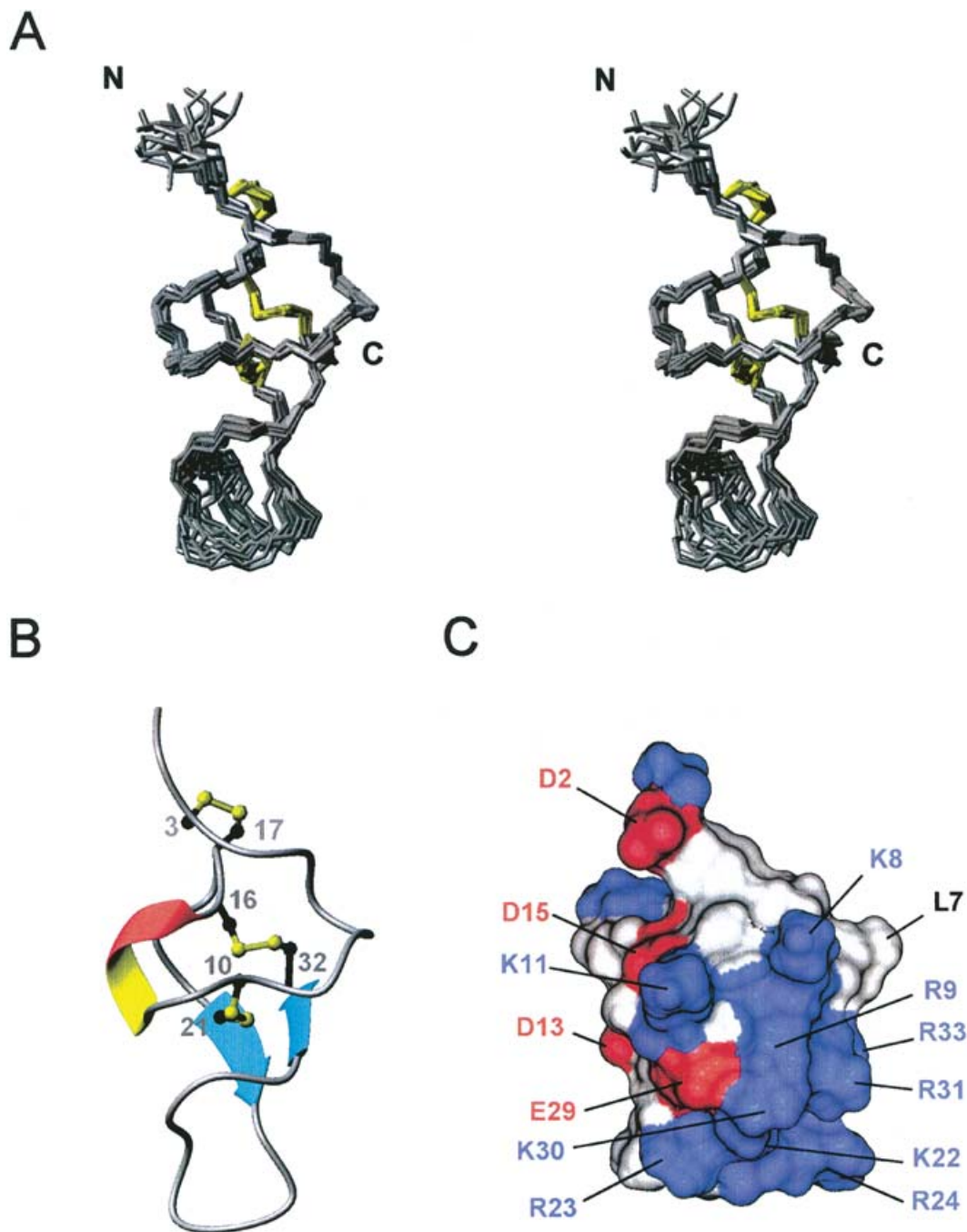


**Figure 3** Solution structure of wIpTx<sub>a</sub>

(A) Stereo view of the heavy atom backbone (N, C<sup>α</sup>, C) for the 20 converged structures of wIpTx<sub>a</sub>, which are superimposed for the best fit over the heavy atom backbone (residues Cys<sup>3</sup>–Arg<sup>23</sup> and residues Lys<sup>30</sup>–Cys<sup>32</sup>). Disulphide bonds are shown in yellow. (B) Schematic diagram of wIpTx<sub>a</sub> illustrating the location of the β-strands (cyan), 3<sub>10</sub>-helical turn (red and yellow) and disulphide bonds (numbered ball and stick in yellow). These Figures were generated using the MOLMOL program [29]. (C) Surface profile of wIpTx<sub>a</sub>. The molecular surface of wIpTx<sub>a</sub> is shown in colour according to the electrostatic potential (negatively charged amino acids are in red, positively charged amino acids are in blue, and uncharged or hydrophobic amino acids are in white). Residues D2, L7, K8, R9, K11, D13, D15, K22, R23, R24, E29, K30, R31 and R33 (single-letter amino acid codes) are indicated.

fingerprint region of the NOESY spectrum, containing sequential  $d_{\alpha N}(i, i + 1)$  connectivity.

For the structure calculation of wIpTx<sub>a</sub>, we used 473 distance constraints derived from the two-dimensional NOESY spectra, 25 dihedral angle constraints derived from the coupling constants and NOE measurements, 12 hydrogen-bond restraints derived from the hydrogen–deuterium exchange experiments

[Cys<sup>10</sup>(HN)–Lys<sup>30</sup>(CO), Lys<sup>20</sup>(HN)–Arg<sup>33</sup>(CO), Lys<sup>22</sup>(HN)–Arg<sup>31</sup>(CO), Arg<sup>31</sup>(HN)–Lys<sup>22</sup>(CO), Cys<sup>32</sup>(HN)–Lys<sup>8</sup>(CO) and Arg<sup>33</sup>(HN)–Lys<sup>20</sup>(CO)] and nine additional disulphide-bond restraints for a total of 519 restraints, corresponding to an average of 15.7 constraints per residue. The disulphide-bond pattern of synthetic wIpTx<sub>a</sub> was determined to be Cys<sup>3</sup>–Cys<sup>17</sup>, Cys<sup>10</sup>–Cys<sup>21</sup> and Cys<sup>16</sup>–Cys<sup>32</sup> by combined approaches of enzyme

**Table 1** Structural statistics for the 20 lowest-energy structures

None of these 20 structures exhibited distance violations > 0.5 Å or dihedral angle violations > 5°.

| Property   | Value             |
|--|-------------------|
| RMS deviations from experimental distance constraints (Å) (494)* | 0.0395 ± 0.0017   |
| RMS deviations from experimental dihedral constraints (°) (25)*  | 0.7879 ± 0.1200   |
| Energetic statistics (kcal · mol <sup>-1</sup> )†                |                   |
| $F_{\text{NOE}}$   | 38.4861 ± 3.2228  |
| $F_{\text{tor}}$   | 0.9821 ± 0.3076   |
| $F_{\text{repel}}$   | 12.9477 ± 2.7362  |
| $E_{\text{L-J}}$   | -61.8040 ± 9.3520 |
| RMS deviations from idealized geometry                           |                   |
| Bonds (Å)  | 0.0036 ± 0.0002   |
| Angles (°)   | 0.6279 ± 0.0198   |
| Impropers (°)  | 0.4603 ± 0.0350   |
| Ramachandran analysis (residues 3–23 and 30–32)‡                 |                   |
| Most favoured regions  | 67.5%             |
| Additionally allowed regions                                     | 31.6%             |
| Generously allowed regions                                       | 0.9%              |
| Disallowed regions   | 0%                |
| Average RMSD (Å)   |                   |
| Backbone (N, C $^{\alpha}$ , C) (residues 3–23 and 30–32)        | 0.38 ± 0.08       |
| All heavy atoms (residues 3–23 and 30–32)                        | 1.46 ± 0.26       |

\* The number of each experimental constraint used in the calculations is given in parentheses.

†  $F_{\text{NOE}}$ ,  $F_{\text{tor}}$  and  $F_{\text{repel}}$  are the energies related to the NOE violations, the torsion angle violations and the van der Waals repulsion term respectively. The values of the force constants used for these terms are the standard values as depicted in the X-PLOR 3.1 manual.  $E_{\text{L-J}}$  is the Lennard–Jones/van der Waals energy calculated with the CHARMM empirical energy function [56].  $E_{\text{L-J}}$  was not used in the dynamic simulated annealing calculations.

‡ The program PROCHECK-NMR was used to assess the stereochemical quality of the structures.

fragmentation and chemical synthesis (C. W. Lee, E. H. Lee, T. Sasaki, K. Sato, K. Takeuchi, H. Takahashi, I. Shimada, D. H. Kim and J. I. Kim, unpublished work).

### Structure description of wIpTx<sub>a</sub>

Twenty structures with the lowest residual restraint violations were used to represent the three-dimensional structure of wIpTx<sub>a</sub> (Figure 3A). These structures have good non-bonded contacts as shown by low Lennard–Jones potential values, and a good covalent geometry, with only small deviations from the ideal bond lengths and bond angles (Table 1). There were no distance or dihedral angle restraint violations greater than 0.5 Å and 5° respectively. Excluding the final two residues of the N-terminus (Gly<sup>1</sup> and Asp<sup>2</sup>) and the loop region from Arg<sup>24</sup> to Glu<sup>29</sup>, both of which were poorly defined by the NMR data, the average root mean square difference (RMSD) for the final 20 structures with respect to the mean co-ordinate positions was 0.38 ± 0.08 Å for the backbone atoms and 1.46 ± 0.26 Å for all heavy atoms. Structural statistics for the 20 converged structures of wIpTx<sub>a</sub> are summarized in Table 1.

The molecular structure of wIpTx<sub>a</sub> consists of two β-strands arranged in an antiparallel fashion, connected by four chain reversals (Figure 3B). The two β-strands are formed by residues Lys<sup>20</sup>–Arg<sup>23</sup> (β-strand I) and Lys<sup>30</sup>–Arg<sup>33</sup> (β-strand II). The first reversal occurs at residues Pro<sup>5</sup>–Lys<sup>8</sup>, which form a type IV β-turn (miscellaneous type). The second and third reversals occur at residues Asp<sup>13</sup>–Asp<sup>15</sup> and Cys<sup>16</sup>–Lys<sup>19</sup> and form a 3<sub>10</sub> helical turn and a type I β-turn respectively. Both of these are contained within the external long loop between the first turn and β-strand I. The final reversal occurs between residues Arg<sup>24</sup> and Glu<sup>29</sup> and

serves to reverse the backbone between β-strands I and II, without showing the characteristic distance pattern of a tight reverse turn. In terms of RMSD, this loop is poorly defined and presents the highest degree of structural disorder in the cysteine-rich region (Figure 3A).

The hydrophobic core of wIpTx<sub>a</sub> is entirely composed of the Cys<sup>10</sup>, Cys<sup>16</sup>, Cys<sup>21</sup> and Cys<sup>32</sup> side chains. The disulphide bond between Cys<sup>10</sup> and Cys<sup>21</sup> connects the second reversal to β-strand I, whereas the disulphide bonds between Cys<sup>3</sup> and Cys<sup>17</sup> and between Cys<sup>16</sup> and Cys<sup>32</sup> connect the third reversal to the N-terminus and β-strand II respectively (Figure 3B). This pattern of disulphide connectivity is topologically classified as an ‘inhibitor cystine knot’ fold [34,35], in which the disulphide bond between Cys<sup>16</sup> and Cys<sup>32</sup> penetrates through a 13-residue ring formed by the peptide backbone and the other two disulphide bonds. Similar topology is frequently found in numerous toxic and inhibitory peptides, including the ω-conotoxins, ω-agatoxins and various protease inhibitors [36–42].

### Structure–activity relationships of IpTx<sub>a</sub>

The biological activities of synthetic wIpTx<sub>a</sub> and its 26 analogues were determined by examining their effects on RyR1 in SR vesicles from rabbit skeletal muscle, using a [<sup>3</sup>H]ryanodine-binding assay. As shown in Figure 4, synthetic wIpTx<sub>a</sub> efficiently increased specific [<sup>3</sup>H]ryanodine binding with EC<sub>50</sub> = 28.40 ± 6.71 nM and B<sub>max</sub> = 6.79 ± 0.30 pmol/mg of protein. The control binding of [<sup>3</sup>H]ryanodine in the absence of wIpTx<sub>a</sub> was 0.57 ± 0.15 pmol/mg of protein. The specific [<sup>3</sup>H]ryanodine binding in the presence of 30 nM of each analogue (corresponding to the apparent EC<sub>50</sub> of wIpTx<sub>a</sub>) is summarized in Figure 4(A). Interestingly, all analogues possessing alanine replacements for basic residues caused an apparent reduction of specific [<sup>3</sup>H]ryanodine binding, whereas all analogues possessing alanine replacements for acidic residues showed slight increases of specific [<sup>3</sup>H]ryanodine binding. In addition, the H6A (His<sup>6</sup> → Ala), L7A, G25A (Gly<sup>25</sup> → Ala), T26A (Thr<sup>26</sup> → Ala) and N27A (Asn<sup>27</sup> → Ala) analogues also showed decreased [<sup>3</sup>H]ryanodine binding. These results suggest that a large surface area on IpTx<sub>a</sub> contributes to activating RyR1, and that the integrity of electrostatic potential, together with other additional factors, affects RyR1 activation.

In order to evaluate the residues essential to RyR1 activation in detail, we examined the dose-dependent activation by all synthetic IpTx<sub>a</sub> analogues further. The EC<sub>50</sub> values of all analogues are summarized in Table 2. Analysis of the dose effects showed that substituting residues at 16 positions, including positions 6, 7, 8, 9, 11, 19, 20, 22, 23, 24, 25, 26, 27, 30, 31 and 33 of IpTx<sub>a</sub> resulted in an important decrease of specific [<sup>3</sup>H]ryanodine binding (Figures 4B, 4C and 4D). In particular, the R24A, R31A and R33A analogues completely abolished specific [<sup>3</sup>H]ryanodine binding to RyR1. Other drastic decreases of specific [<sup>3</sup>H]ryanodine binding were observed with L7A, K22A and R23A analogues (Figure 4D). In the case of acidic residues, alanine replacement resulted in slightly decreased EC<sub>50</sub> values, indicating that the negatively charged residues in IpTx<sub>a</sub> slightly obstruct the ability of the toxin molecule to activate RyR1. The CD spectral analyses showed that the conformations of the alanine-scanning analogues were almost identical with that of wIpTx<sub>a</sub> (Figure 1), except for the single case of the linear analogue (Ala<sup>3,10,16,17,21,32</sup>)IpTx<sub>a</sub>, which displayed completely abolished activity (Figure 4D).

Previously, Gurrola et al. [17] reported that the mutations of Arg<sup>23</sup> (R23E) and Thr<sup>26</sup> (T26A and T26E) in IpTx<sub>a</sub> decreased the capacity of IpTx<sub>a</sub> to activate RyR1, and suggested that in IpTx<sub>a</sub>, a

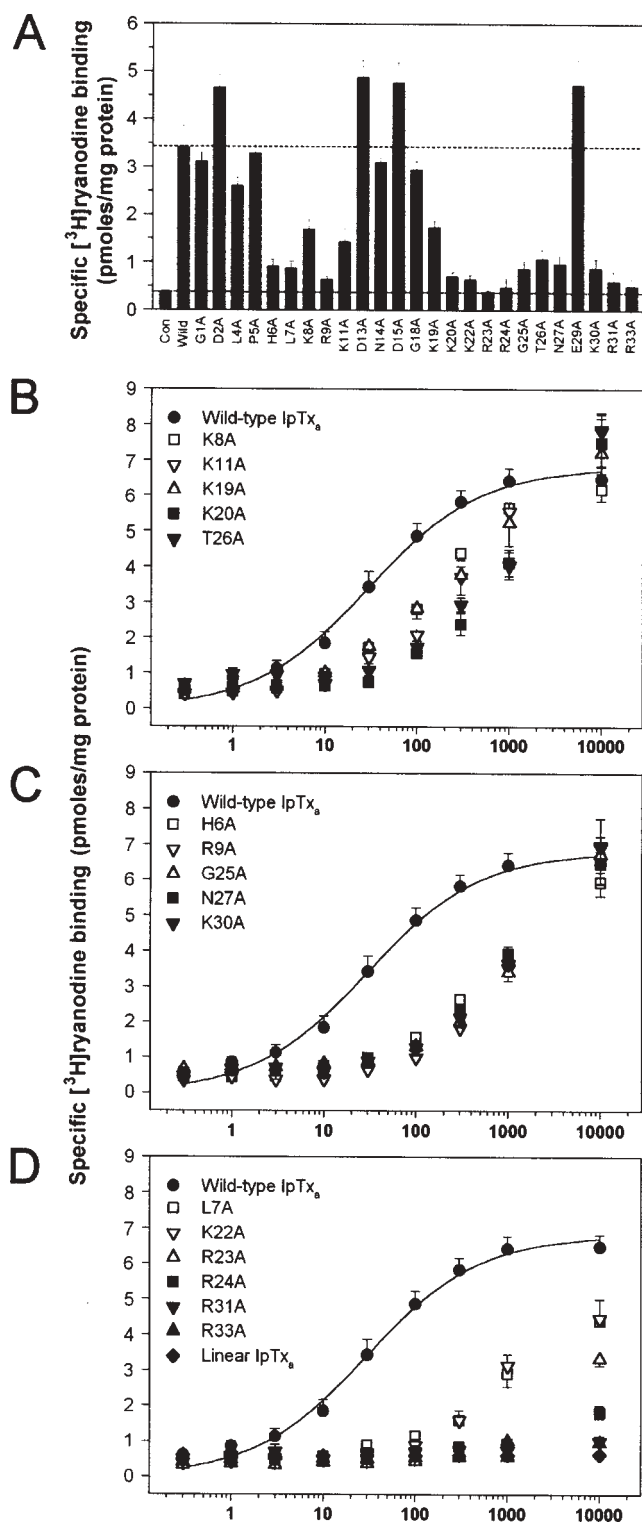


**Figure 4** Activity measurements of wIpTx<sub>a</sub> and alanine-scanning analogues calculated with the [<sup>3</sup>H]ryanodine binding assay

(A) Con and Wild are specific [<sup>3</sup>H]ryanodine binding to RyR1 in the absence ( $0.38 \pm 0.01$  pmol/mg) and presence ( $3.44 \pm 0.43$  pmol/mg) of wIpTx<sub>a</sub> (30 nM) respectively. The values are the means  $\pm$  S.E.M. of five independent experiments. (B)–(D) Dose-dependent activation of [<sup>3</sup>H]ryanodine binding to RyR1 by wIpTx<sub>a</sub> and its analogues. The effect of wIpTx<sub>a</sub> on [<sup>3</sup>H]ryanodine binding was compared with that of K8A, K11A, K19A, K20A and T26A (B), H6A, R9A, G25A, N27A and K30A (C), L7A, K22A, R23A, R24A, R31A, R33A and the linear analogue [(Ala<sup>3,10,16,17,21,32</sup>)IpTx<sub>a</sub>] (D). The values are means  $\pm$  S.E.M. of five independent replicates. Single-letter amino acid codes are used for the mutations.

**Table 2** EC<sub>50</sub> values of wIpTx<sub>a</sub> and analogues

The data are means  $\pm$  S.E.M. of five replicated experiments (see the Materials and methods section). + and – indicate the alanine-scanning analogue of positively and negatively charged residues of IpTx<sub>a</sub> respectively.

| Analyte   | EC <sub>50</sub> (nM)  |
|-----------|------------------------|
| Wild-type | 28.40 $\pm$ 6.71       |
| G1A       | 33.40 $\pm$ 4.83       |
| D2A       | 12.20 $\pm$ 2.17       |
| L4A       | 54.75 $\pm$ 7.79       |
| P5A       | 40.57 $\pm$ 5.18       |
| H6A       | 588.46 $\pm$ 71.24     |
| L7A       | 2769.22 $\pm$ 591.42   |
| K8A       | 130.53 $\pm$ 15.97     |
| R9A       | 727.58 $\pm$ 112.50    |
| K11A      | 193.90 $\pm$ 34.72     |
| D13A      | 9.21 $\pm$ 2.66        |
| N14A      | 32.25 $\pm$ 4.45       |
| D15A      | 10.40 $\pm$ 1.05       |
| G18A      | 33.07 $\pm$ 5.14       |
| K19A      | 140.97 $\pm$ 24.93     |
| K20A      | 480.36 $\pm$ 92.21     |
| K22A      | 1985.72 $\pm$ 383.56   |
| R23A      | 11884.93 $\pm$ 2767.73 |
| R24A      | > 1 000 000            |
| G25A      | 680.52 $\pm$ 194.31    |
| T26A      | 327.12 $\pm$ 104.41    |
| N27A      | 570.52 $\pm$ 124.22    |
| E29A      | 12.06 $\pm$ 1.30       |
| K30A      | 615.88 $\pm$ 130.13    |
| R31A      | > 1 000 000            |
| R33A      | > 1 000 000            |
| Linear*   | > 1 000 000            |

\* Linear analogue [(Ala<sup>3,10,16,17,21,32</sup>)IpTx<sub>a</sub>] was created by replacing all six cysteine residues with alanines.

cluster of basic residues (Lys<sup>19</sup>–Arg<sup>24</sup>) followed by Thr<sup>26</sup> mimics the II–III loop of the DHPR  $\alpha$ -subunit and is important for binding to RyR1. This agrees in part with our findings from analysis of analogues with alanine replacement of Arg<sup>23</sup> and Thr<sup>26</sup>. Through a series of dose-dependent experiments using a complete set of alanine-scanning analogues, however, we found that most critical residues responsible for RyR1 activation (Arg<sup>24</sup>, Arg<sup>31</sup> and Arg<sup>33</sup>, together with residues Lys<sup>22</sup> and Arg<sup>23</sup>) are located within the C-terminal region of IpTx<sub>a</sub>. In addition, Leu<sup>7</sup> is of great importance, as it serves as a hydrophobic partner in the specific interaction with RyR1 (Figure 4D). The three-dimensional IpTx<sub>a</sub> structure shows that these six essential residues, together with other several important residues (His<sup>6</sup>, Lys<sup>8</sup>, Arg<sup>9</sup>, Lys<sup>11</sup>, Lys<sup>19</sup>, Lys<sup>20</sup>, Gly<sup>25</sup>, Thr<sup>26</sup>, Asn<sup>27</sup> and Lys<sup>30</sup>), are clustered together on one surface of the toxin molecule (an area of approx. 1900 Å<sup>2</sup>) (Figure 5B). This region forms a functional surface with a putative binding site that probably interacts with the RyR1 cytoplasmic region. Interestingly, the opposite site is rich in acidic residues (Asp<sup>2</sup>, Asp<sup>13</sup>, Asp<sup>15</sup> and Glu<sup>29</sup>), and it forms a striking contrast with the positively charged functional surface (Figure 3C).

### Structural comparisons with Mca and peptide A

In addition to IpTx<sub>a</sub>, another exogenous ligand derived from scorpion venom mimics the effect of peptide A on RyR1. Mca, a 33-mer peptide toxin isolated from the venom of *Scorpio maurus*, activates RyR1 and shares 82% sequence identity with IpTx<sub>a</sub> [43]. As expected from this high degree of sequence identity,

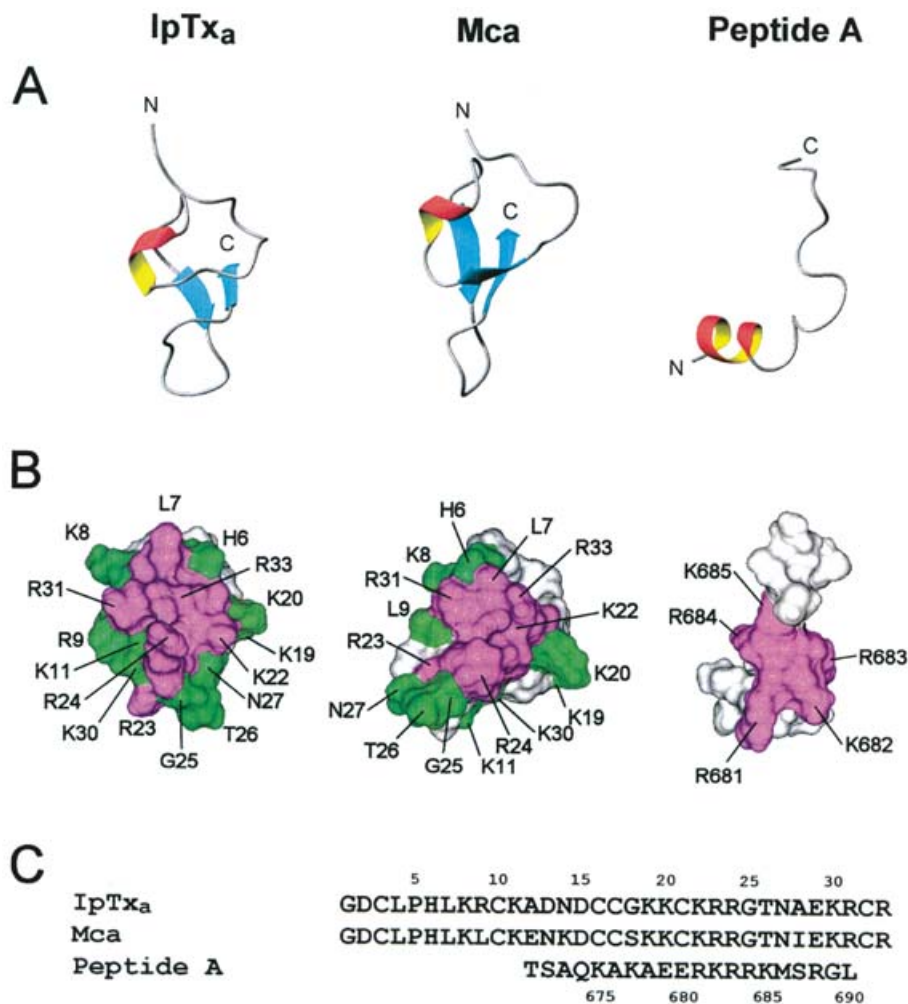


**Figure 5** Structural comparison of IpTx<sub>a</sub>, Mca (PDB code, 1C6W) and peptide A (PDB code, 1DU1)

(A) Schematic diagrams of IpTx<sub>a</sub>, Mca and peptide A illustrating the location of the  $\beta$ -strands (cyan) and  $3_{10}$ -helical turn (red and yellow). (B) Surface profiles of IpTx<sub>a</sub>, Mca and peptide A. For comparison, amino acids involved in the function of these peptides are emphasized in colour. Corresponding amino acids in Mca and peptide A, six essential amino acids (L7, K22, R23, R24, R31 and R33) of IpTx<sub>a</sub> and maurocalcine, and the R681–K685 region of peptide A are shown in purple; ten functionally important residues (H6, K8, R9, K11, K19, K20, G25, T26, N27 and K30) of IpTx<sub>a</sub> and maurocalcine are shown in green. Single-letter amino acid codes are used. (C) Comparative arrangements of the amino acid sequences of IpTx<sub>a</sub>, Mca and peptide A.

both scorpion toxins present a similar overall molecular fold in solution. Mosbah et al. [44] determined the NMR solution structure of Mca, showing that it consists of three  $\beta$ -strands and four chain reversals. This report suggested that the three-dimensional surface of Mca has a unique charge distribution with a marked anisotropy that emerges from the molecule through its basic surface. Such a dipole moment is also observed in the surface profile of IpTx<sub>a</sub> (Figure 3C). IpTx<sub>a</sub> is the same length as Mca, and the two differ by only six amino acid residues: those at positions 9, 12, 13, 14, 18 and 28. Except for the Arg<sup>9</sup> residue, all residues of IpTx<sub>a</sub> that are important to RyR1 activation are well conserved in the primary and tertiary structures of Mca (Figure 5B), enclosing a slightly decreased functional surface area of approx. 1600 Å<sup>2</sup>. Thus it would be reasonable to expect both scorpion toxins to have a similar binding affinity for a common site on RyR1 that is important for skeletal muscle E–C coupling. However, it should be noted that these scorpion toxins have different levels of effect on RyR1 gating, which undergoes a reversible transition between subconductance and fast gating states. Although both toxins may share a binding site on RyR1, IpTx<sub>a</sub> and Mca induce

subconductances that correspond to 28% and 48%, respectively, of the native full conductance at the positive holding potential [43,45]. This result seems to imply that a small change in the local charge distribution, due to variation of six amino acids, may induce slightly different substates in toxin gating of RyR1.

A major structural difference between IpTx<sub>a</sub> and Mca is found near the N-terminus, where Mca forms an additive peripheral  $\beta$ -strand (residues 9–11) that participates in the triple-stranded  $\beta$ -sheet (Figure 5A), but the corresponding sequence of IpTx<sub>a</sub> consists of only a single residue (Cys<sup>10</sup>) that is hydrogen-bonded to the central  $\beta$ -strand. Interestingly, the first residue (Leu<sup>9</sup>) of  $\beta$ -strand I in Mca joins with the side-chains of Cys<sup>10</sup>, Cys<sup>16</sup>, Cys<sup>21</sup> and Cys<sup>32</sup> to form the molecule's hydrophobic core. In IpTx<sub>a</sub>, this residue is replaced by a positively charged arginine that plays a functional role in RyR1 activation. It is thus likely that some variations in amino acid sequences between IpTx<sub>a</sub> and Mca are to meet the structural and/or functional requirements of toxin molecules that evolve from different venomous sources.

In contrast, the solution conformation of the peptide A segment from the II–III loop of skeletal DHPR distinctly differs from that

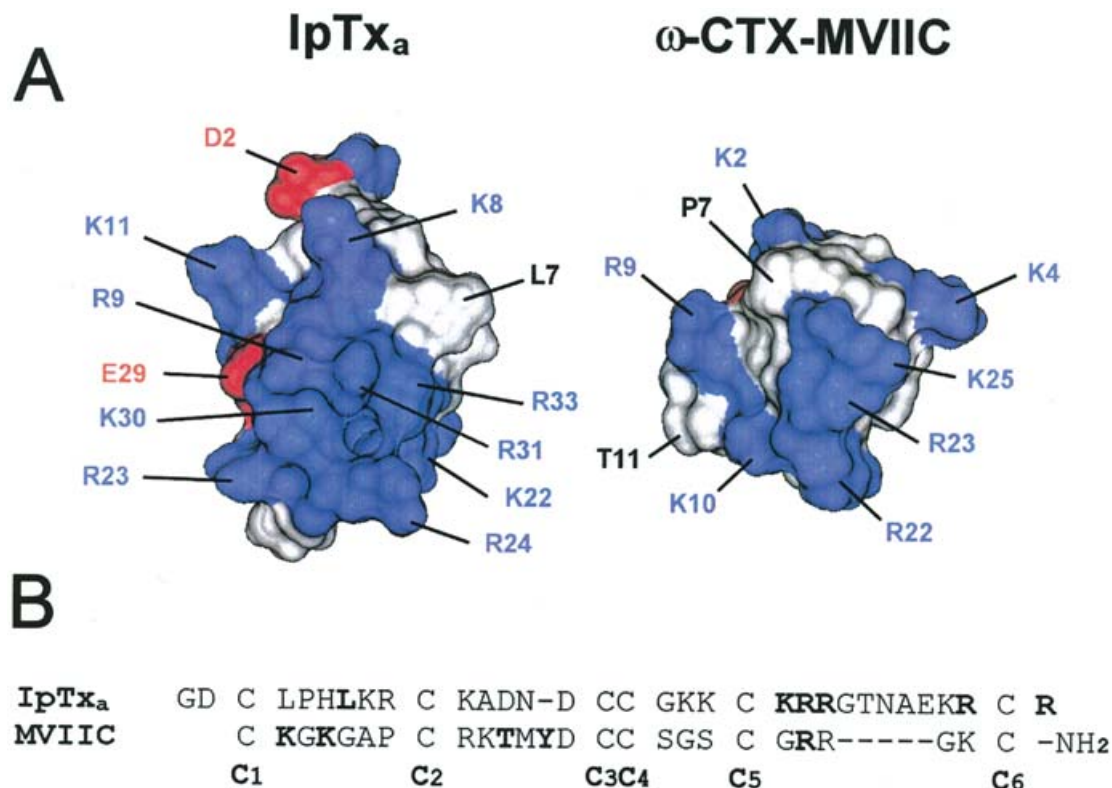


**Figure 6** Structural comparison of IpTx<sub>a</sub> and ω-CTX-MVIIC

(A) Comparison between surface profiles of IpTx<sub>a</sub> and ω-CTX-MVIIC (PDB code 1CNN). The colour codes are the same as those in Figure 3(C). The molecules are oriented with the positively charged amino acid cluster of each molecule in a certain plane. (B) Amino acids in the active sites of IpTx<sub>a</sub> and MVIIC are emboldened in their primary sequence alignments.

of IpTx<sub>a</sub> [46]. As shown in Figure 5(A), the structure of peptide A consists of a helical segment extending from the N-terminus to residue Lys<sup>685</sup>, which is followed by a disordered region that extends through to the C-terminus. Despite this structural difference, these peptide activators show a distinct similarity in the spatial orientation of active residues necessary to target the common binding site on RyR1. It was previously reported that the peptide A-related segment (Glu<sup>666</sup>–Leu<sup>690</sup>) might bind to the same site as IpTx<sub>a</sub> on RyR1 [17]. In terms of competitive binding, peptide A presents a basic surface profile with the five consecutive residues (Arg<sup>681</sup>–Lys<sup>685</sup>) clustered at the C-terminal end of the α-helix, whereas IpTx<sub>a</sub> presents similar positively charged residues (Lys<sup>22</sup>, Arg<sup>23</sup>, Arg<sup>24</sup>, Arg<sup>31</sup> and Arg<sup>33</sup>) aligned in a central region (Figure 5B). In both peptides, these basic surfaces are fully exposed to the solvent and present a characteristic shape that may be directly involved in the RyR1 activation important for skeletal muscle E–C coupling. Together, these observations may explain, at least in part, how IpTx<sub>a</sub> and peptide A compete for a common binding site on the RyR1 channel protein.

However, although both use a common binding site, the affinities of IpTx<sub>a</sub> and peptide A for RyR1 differ. IpTx<sub>a</sub> activates RyR1 with a high nanomolar affinity, whereas peptide A activates RyR1 with a lower micromolar affinity [17]. As summarized in Table 2, the EC<sub>50</sub> values for the IpTx<sub>a</sub> alanine-scanning analogues varied considerably depending on the location of the substitution. [<sup>3</sup>H]Ryanodine binding to RyR1 was significantly reduced following alanine replacement of all tested basic residues, including the five critical residues (Lys<sup>22</sup>, Arg<sup>23</sup>, Arg<sup>24</sup>, Arg<sup>31</sup> and Arg<sup>33</sup>), and several other residues (His<sup>6</sup>, Leu<sup>7</sup>, Gly<sup>25</sup>, Thr<sup>26</sup> and Asn<sup>27</sup>), indicating that amino acid residues involved in RyR1

activation make up over the half of the toxin molecule with the exception of cysteine residues. In contrast, the functional surface of peptide A includes only five consecutive basic residues (Arg<sup>681</sup>, Lys<sup>682</sup>, Arg<sup>683</sup>, Arg<sup>684</sup> and Lys<sup>685</sup>) that are clustered at the C-terminal end of the α-helix. In three dimensions, IpTx<sub>a</sub> exhibits a large functional surface area, approx. 1900 Å<sup>2</sup>, whereas peptide A bears a much smaller functional surface area, approx. 800 Å<sup>2</sup>.

In measurements of single channel currents, IpTx<sub>a</sub> induced a long-lived subconductance state in RyR1 that possessed 28 % of the characteristic full open state at the positive holding potential. In contrast, peptide A induced long-lived channel closures with occasional burst transitions to subconductance states of 65 % or 86 % of the full conductance, indicating that IpTx<sub>a</sub> and peptide A stabilize distinct RyR1 gating states through somewhat different interaction mechanisms [47].

Overall, these results suggest that the site where peptide A binds to RyR1 belongs to a subset of macrosites capable of being occupied by IpTx<sub>a</sub>, resulting in differing the affinity and the mode of activation.

#### Structural comparison with ω-CTX-MVIIC, a voltage-gated P/Q-type Ca<sup>2+</sup> channel blocker

Voltage-gated Ca<sup>2+</sup> channels are classified into several subtypes, which include the L-, N-, P-, Q-, R- and T-subtypes, according to their electrophysiological and pharmacological properties [48]. ω-CTXs are highly potent blockers of voltage-gated Ca<sup>2+</sup> channels and are useful ligands for the pharmacological discrimination of Ca<sup>2+</sup> channel subtypes [49]. Extensive structure–activity



studies have revealed that all  $\omega$ -CTXs (e.g.  $\omega$ -CTX-GVIA and -MVIIA, N-type  $\text{Ca}^{2+}$ -channel blockers, and the  $\omega$ -CTX-MVIIC, P/Q-type  $\text{Ca}^{2+}$ -channel blocker) share significant structural similarity in three dimensions, but possess distinct functional sites responsible for the specific interaction with individual voltage-gated  $\text{Ca}^{2+}$  channel subtypes [50–53]. The molecular architecture of the cone-snail  $\omega$ -CTXs is entirely composed of an ‘inhibitor cystine knot’ fold constrained by three intramolecular disulphide bonds. This structure is also found in the RyR1-targeting scorpion toxins IpTx<sub>a</sub> and Mca, indicating that the  $\omega$ -scaffold is a general molecular topology of exogenous toxins targeting the  $\text{Ca}^{2+}$  channels.

Among  $\omega$ -CTXs,  $\omega$ -CTX-MVIIC is the most structurally similar to the scorpion RyR1 activators. As shown in Figure 6(A),  $\omega$ -CTX-MVIIC exhibits a highly basic structural surface that includes several positively charged amino acid residues. Although there is a high degree of structural similarity between IpTx<sub>a</sub> and  $\omega$ -CTX-MVIIC, the two  $\text{Ca}^{2+}$ -channel-targeting toxins show no cross-reactivity; IpTx<sub>a</sub> has no affinity for the P/Q-type  $\text{Ca}^{2+}$  channel and  $\omega$ -CTX-MVIIC has no affinity for the RyR1 [17]. This suggests that the two toxins form distinct functional sites responsible for the specific interaction with each channel protein [53]. The functionally important residues of IpTx<sub>a</sub> for the binding to RyR1 consist of five protruding basic residues (Lys<sup>22</sup>, Arg<sup>23</sup>, Arg<sup>24</sup>, Arg<sup>31</sup> and Arg<sup>33</sup>) and one hydrophobic residue (Leu<sup>7</sup>), with approx. ten additional residues assisting. In contrast, the functional residues for  $\omega$ -CTX-MVIIC action on the P/Q-type  $\text{Ca}^{2+}$  channel include three basic residues (Lys<sup>2</sup>, Lys<sup>4</sup> and Arg<sup>22</sup>) and two polar residues (Thr<sup>11</sup> and Tyr<sup>13</sup>) [53], suggesting that IpTx<sub>a</sub> forms a larger functional surface than does  $\omega$ -CTX-MVIIC.  $\omega$ -CTX-MVIIC is shorter in length than IpTx<sub>a</sub>, and its positively charged surface area is also smaller than that of IpTx<sub>a</sub>, mainly due to fewer basic amino acids between the fifth cysteine and the C-terminus (three compared with six) (Figure 6B). In IpTx<sub>a</sub>, this region forms a long hairpin loop with an electropositive potential, incorporating  $\beta$ -strands I and II (Figure 3B). As previously mentioned, both IpTx<sub>a</sub> and peptide A share a necessary alignment of five basic residues that act at a common site on RyR1 (Figure 5B).  $\omega$ -CTX-MVIIC also possesses a similar basic structural region, consisting of five basic residues (Arg<sup>9</sup>, Lys<sup>10</sup>, Arg<sup>22</sup>, Arg<sup>23</sup> and Lys<sup>25</sup>) (Figure 6A), but its shape is relatively different from that of both IpTx<sub>a</sub> and peptide A, resulting in a failure to activate RyR1. Taken together, these observations suggest that the correct distribution of surface charges is important to specific interaction with RyR1, rather than the globular structure maintained by the conserved disulphide framework. This may be one reason why  $\omega$ -CTX-MVIIC does not compete for the same binding site as IpTx<sub>a</sub> and peptide A, thus providing structural and molecular insights into the specific interaction mode of RyR1-targeting peptide effectors.

## Conclusion

In the present study, we have determined the NMR solution structure of the peptide activator IpTx<sub>a</sub>, and identified the functional surface that is responsible for its high-affinity interaction with RyR1. A detailed comparison between IpTx<sub>a</sub> and peptide A revealed that the existence of complementary surface profiles, created by different molecular scaffolds, is limited between the C-terminal  $\beta$ -sheet region of IpTx<sub>a</sub> and the  $\alpha$ -helical end region of peptide A. Thus it seems that the site where peptide A binds to RyR1 belongs to a subset of the macrosites occupied by IpTx<sub>a</sub>, resulting in differing affinities and subconductance states. A comparative surface analysis with  $\omega$ -CTX-MVIIC suggests that the

characteristic shape of positively charged binding surface rather than globular shape is responsible for the specific interaction of RyR1-targeting peptide effectors. Taken together, these structural and functional studies on ryanodine-sensitive channel effectors, together with our knowledge of the three-dimensional structure of DHPR and RyR1 obtained previously by cryo-electron microscopy and image processes [54,55], open up a new avenue for the elucidation of the molecular details of skeletal type E–C coupling.

This study was supported by grants from the Korean Ministry of Science and Technology (Critical Technology 21.00-J-LF-01-B-54), the Korea Science and Engineering Foundation through the Research Center for Proteinaceous Materials (The Ministry of Science and Technology). C. W. L. and E. H. L. are supported in part by the Korean Ministry of Education (Brain Korea 21 programme).

## REFERENCES

- Bers, D. M. (1991) Excitation–Contraction Coupling and Cardiac Contractile Force, Kluwer Academic Publishers, Dordrecht
- Nabauer, M., Callewaert, G., Cleemann, L. and Morad, M. (1989) Regulation of calcium release is gated by calcium current, not gating charge, in cardiac myocytes. *Science* **244**, 800–803
- Armstrong, C. M., Bezanila, F. M. and Horowitz, P. (1972) Twitches in the presence of ethylene glycol bis-(aminoethyl ether)-N,N'-tetracetic acid. *Biochim. Biophys. Acta* **267**, 605–608
- Marty, I., Robert, M., Villaz, M., De Jongh, K. S., Lai, Y., Catterall, W. A. and Ronjat, M. (1994) Biochemical evidence for a complex involving dihydropyridine receptor and ryanodine receptor in triad junctions of skeletal muscle. *Proc. Natl. Acad. Sci. U.S.A.* **91**, 2270–2274
- Tanabe, T., Beam, K. G., Adams, B. A., Niidome, T. and Numa, S. (1990) Regions of the skeletal muscle dihydropyridine receptor critical for excitation–contraction coupling. *Nature (London)* **346**, 567–569
- Lu, X., Xu, L. and Meissner, G. (1994) Activation of the skeletal muscle calcium release channel by a cytoplasmic loop of the dihydropyridine receptor. *J. Biol. Chem.* **269**, 6511–6516
- El-Hayek, R., Antoniu, B., Wang, J., Hamilton, S. L. and Ikemoto, N. (1995) Identification of calcium release-triggering and blocking regions of the II–III loop of the skeletal muscle dihydropyridine receptor. *J. Biol. Chem.* **270**, 22116–22118
- Nakai, J., Dirksen, R. T., Nguyen, H. T., Pessah, I. N., Beam, K. G. and Allen, P. D. (1996) Enhanced dihydropyridine receptor channel activity in the presence of ryanodine receptor. *Nature (London)* **380**, 72–75
- Slavik, K. J., Wang, J. P., Aghdasi, B., Zhang, J. Z., Mandel, F., Malouf, N. and Hamilton, S. L. (1997) A carboxy-terminal peptide of the  $\alpha$ 1-subunit of the dihydropyridine receptor inhibits  $\text{Ca}^{2+}$  release channels. *Am. J. Physiol.* **272**, C1475–C1481
- Leong, P. and MacLennan, D. H. (1998) The cytoplasmic loops between domains II and III and domains III and IV in the skeletal muscle dihydropyridine receptor bind to a contiguous site in the skeletal muscle ryanodine receptors. *J. Biol. Chem.* **273**, 29958–29964
- Grabner, M., Dirksen, R. T., Suda, N. and Beam, K. G. (1999) The II–III loop of the skeletal muscle dihydropyridine receptor is responsible for the bi-directional coupling with the ryanodine receptor. *J. Biol. Chem.* **274**, 21913–21919
- Sencer, S., Papineni, R. V., Halling, D. B., Pate, P., Krol, J., Zhang, J. Z. and Hamilton, S. L. (2001) Coupling of RYR1 and L-type calcium channels via calmodulin binding domains. *J. Biol. Chem.* **276**, 38237–38241
- Nakai, J., Sekiguchi, N., Rando, T. A., Allen, P. D. and Beam, K. G. (1998) Two regions of the ryanodine receptor involved in coupling with L-type  $\text{Ca}^{2+}$  channels. *J. Biol. Chem.* **273**, 13403–13406
- El-Hayek, R., Lokuta, A. J., Arevalo, C. and Valdivia, H. H. (1995) Peptide probe of ryanodine receptor function. *J. Biol. Chem.* **270**, 28696–28704
- Zamudio, F. Z., Gurrrola, G. B., Arevalo, C., Sreekumar, R., Walker, J. W., Valdivia, H. H. and Possani, L. D. (1997) Primary structure and synthesis of Imperatoxin A (IpTx<sub>a</sub>), a peptide activator of  $\text{Ca}^{2+}$  release channels/ryanodine receptors. *FEBS Lett.* **405**, 385–389
- El-Hayek, R. and Ikemoto, N. (1998) Identification of the minimum essential region in the II–III loop of the dihydropyridine receptor 1 subunit required for activation of skeletal muscle-type excitation–contraction coupling. *Biochemistry* **37**, 7015–7020
- Gurrrola, G. B., Arevalo, C., Sreekumar, R., Lokuta, A. J., Walker, J. W. and Valdivia, H. H. (1999) Activation of ryanodine receptors by imperatoxin A and a peptide segment of the II–III loop of the dihydropyridine receptor. *J. Biol. Chem.* **274**, 7879–7886

- 18 Green, D., Pace, S., Curtis, S. M., Sakowska, M., Lamb, G. D., Dulhunty, A. F. and Casarotto, M. G. (2003) The three-dimensional structural surface of two  $\beta$ -sheet scorpion toxins mimics that of an  $\alpha$ -helical dihydropyridine receptor segment. *Biochem. J.* **370**, 517–527
- 19 Rance, M., Sørensen, O. W., Bodenhausen, G., Wagner, G., Ernst, R. R. and Wüthrich, K. (1983) Improved spectral resolution in COSY  $^1\text{H}$  NMR spectra of protein via double quantum filtering. *Biochem. Biophys. Res. Commun.* **117**, 479–485
- 20 Griesinger, C., Sørensen, O. W. and Ernst, R. R. (1987) Practical aspects of the E.COSY technique: measurement of scalar spin–spin coupling constants in peptides. *J. Magn. Reson.* **75**, 474–492
- 21 Bax, A. and Davis, D. G. (1985) MLEV-17-based two-dimensional homonuclear magnetization transfer spectroscopy. *J. Magn. Reson.* **65**, 355–360
- 22 Jeener, J., Meier, B. N., Bachmann, P. and Ernst, R. P. (1979) Investigation of exchange processes by two-dimensional NMR spectroscopy. *J. Chem. Phys.* **71**, 4546–4553
- 23 Wüthrich, K., Billeter, M. and Braun, W. (1983) Pseudo-structures for the 20 common amino acids for use in studies of protein conformations by measurement of intramolecular proton–proton distance constraints with nuclear magnetic resonance. *J. Mol. Biol.* **169**, 949–961
- 24 Clore, M., Gronenborn, A. M., Nilges, M. and Ryan, C. A. (1987) Three-dimensional structure of potato carboxypeptidase inhibitor in solution: a study using nuclear magnetic resonance, distance geometry and restraint molecular dynamics. *Biochemistry* **26**, 8012–8023
- 25 Nilges, M., Gronenborn, A. M., Brünger, A. T. and Clore, G. M. (1988) Determination of three-dimensional structures of proteins by simulated annealing with interproton distance restraints: application to crambin, potato carboxypeptidase inhibitor and barley serine proteinase inhibitor 2. *Protein Eng.* **2**, 27–38
- 26 Brünger, A. T. (1993) X-PLOR Manual, Version 3.1, Yale University, New Haven
- 27 Laskowski, R. A., Rullmann, J. A., MacArthur, M. W., Kaptein, R. and Thornton, J. M. (1996) AQUA and PROCHECK-NMR: programs for checking the quality of protein structures solved by NMR. *J. Biomol. NMR* **8**, 477–486
- 28 Hutchinson, E. G. and Thornton, J. M. (1996) PROMOTIF – a program to identify and analyze structural motifs in proteins. *Protein Sci.* **5**, 212–220
- 29 Koradi, R., Billeter, M. and Wüthrich, K. (1996) MOLMOL: a program for display and analysis of macromolecular structures. *J. Mol. Graph.* **14**, 29–32
- 30 Kim, D. H., Sreter, F. A., Ohnishi, S. T., Ryan, J. F., Roberts, J., Allen, P. D., Meszaros, L. G., Antonia, B. and Ikemoto, N. (1984) Kinetic studies of  $\text{Ca}^{2+}$  release from sarcoplasmic reticulum of normal and malignant hyperthermia susceptible pig muscles. *Biochim. Biophys. Acta* **775**, 320–327
- 30a Bradford, M. M. (1976) A rapid and sensitive method for the quantitation of microgram quantities of protein utilizing the principle of protein-dye binding. *Anal. Biochem.* **72**, 248–254
- 31 Campbell, K. P., Knudson, C. M., Imagawa, T., Leung, A. T., Sutko, J. L., Kahl, S. D., Raab, C. R. and Madson, L. (1987) Identification and characterization of the high affinity [ $^3\text{H}$ ]ryanodine receptor of the junctional sarcoplasmic reticulum  $\text{Ca}^{2+}$  release channel. *J. Biol. Chem.* **262**, 6460–6463
- 32 Kim, D. H., Mkparu, F., Kim, C. R. and Carroll, R. F. (1994) Alteration of  $\text{Ca}^{2+}$  release channel function in sarcoplasmic reticulum of pressure-overload-induced hypertrophic rat heart. *J. Mol. Cell. Cardiol.* **26**, 1505–1512
- 33 Wüthrich, K. (1986) *NMR of Proteins and Nucleic Acids*, John Wiley and Sons, Inc., New York
- 34 Pallaghy, P. K., Nielsen, K. J., Craik, D. J. and Norton, R. S. (1994) A common structural motif incorporating a cystine knot and a triple-stranded  $\beta$ -sheet in toxic and inhibitory polypeptides. *Protein Sci.* **3**, 1833–1839
- 35 Norton, R. S. and Pallaghy, P. K. (1998) The cystine knot structure of ion channel toxins and related polypeptides. *Toxicon* **36**, 1573–1583
- 36 Davis, J. H., Bradley, E. K., Miljanich, G. P., Nadasdi, L., Ramachandran, J. and Basus, V. J. (1993) Solution structure of omega-conotoxin GVIA using 2-D NMR spectroscopy and relaxation matrix analysis. *Biochemistry* **32**, 7396–7405
- 37 Pallaghy, P. K., Duggan, B. M., Pennington, M. W. and Norton, R. S. (1993) Three-dimensional structure in solution of the calcium channel blocker  $\omega$ -conotoxin. *J. Mol. Biol.* **234**, 405–420
- 38 Kohno, T., Kim, J. I., Kobayashi, K., Kodera, Y., Maeda, T. and Sato, K. (1995) Three-dimensional structure in solution of the calcium channel blocker  $\omega$ -conotoxin MVIIA. *Biochemistry* **34**, 10256–10265
- 39 Kim, J. I., Konishi, S., Iwai, H., Kohno, T., Gouda, H., Shimada, I., Sato, K. and Arata, Y. (1995) Three-dimensional solution structure of the calcium channel antagonist  $\omega$ -agatoxin IVA: consensus molecular folding of calcium channel blockers. *J. Mol. Biol.* **250**, 659–671
- 40 Reily, M. D., Thanabal, V. and Adams, M. E. (1995) The solution structure of  $\omega$ -Aga-IVB, a P-type calcium channel antagonist from venom of the funnel web spider, *Agelenopsis aperta*. *J. Biomol. NMR* **5**, 122–132
- 41 Saether, O., Craik, D. J., Campbell, I. D., Sletten, K., Juul, J. and Morman, D. G. (1995) Elucidation of the primary and three-dimensional structure of the uterotonic polypeptide kalata B1. *Biochemistry* **34**, 4147–4158
- 42 Nilges, M., Habazettl, J., Brünger, A. T. and Holak, T. A. (1991) Relaxation matrix refinement of the solution structure of squash trypsin inhibitor. *J. Mol. Biol.* **248**, 106–124
- 43 Fajloun, Z., Kharrat, R., Chen, L., Lecomte, C., Di Luccio, E., Bichet, D., El Ayeb, M., Rochat, H., Allen, P. D., Pessah, I. N. et al. (2000) Chemical synthesis and characterization of maurocalcine, a scorpion toxin that activates  $\text{Ca}^{2+}$  release channel/ryanodine receptors. *FEBS Lett.* **469**, 179–185
- 44 Mosbah, A., Kharrat, R., Fajloun, Z., Renisio, J. G., Blanc, E., Sabatier, J. M., El Ayeb, M. and Darbon, H. (2000) A new fold in the scorpion toxin family, associated with an activity on a ryanodine-sensitive calcium channel. *Proteins* **40**, 436–442
- 45 Tripathy, A., Resch, W., Xu, L., Valdivia, H. H. and Meissner, G. (1998) Imperatoxin A induces subconductance states in  $\text{Ca}^{2+}$  release channels (ryanodine receptors) of cardiac and skeletal muscle. *J. Gen. Physiol.* **111**, 679–690
- 46 Casarotto, M. G., Gibson, F., Pace, S. M., Curtis, S. M., Mulcair, M. and Dulhunty, A. F. (2000) A structural requirement for activation of skeletal ryanodine receptors by peptides of the dihydropyridine receptor II–III loop. *J. Biol. Chem.* **275**, 11631–11637
- 47 Chen, L., Esteve, E., Sabatier, J. M., Ronjat, M., Waard, M. D., Allen, P. D. and Pessah, I. N. (2003) Maurocalcine and peptide A stabilize distinct subconductance states of ryanodine receptor type 1 (RyR1) revealing a proportional gating mechanism. *J. Biol. Chem.* **278**, 16095–16106
- 48 Snutch, T. P. and Reiner, P. B. (1992)  $\text{Ca}^{2+}$  channels: diversity of form and function. *Curr. Opin. Neurobiol.* **2**, 247–253
- 49 Olivera, B. M., Miljanich, G. P., Ramachandran, J. and Adams, M. E. (1994) Calcium channel diversity and neurotransmitter release: the  $\omega$ -conotoxins and  $\omega$ -agatoxins. *Annu. Rev. Biochem.* **63**, 823–867
- 50 Kim, J. I., Takahashi, M., Ogura, A., Kohno, T., Kudo, Y. and Sato, K. (1994) Hydroxyl group of Tyr $^{13}$  is essential for the activity of  $\omega$ -conotoxin GVIA, a peptide toxin for N-type calcium channel. *J. Biol. Chem.* **269**, 23876–23878
- 51 Kim, J. I., Takahashi, M., Ohtake, A., Wakamiya, A. and Sato, K. (1995) Tyr $^{13}$  is essential for the activity of  $\omega$ -conotoxin MVIIA and GVIA, specific N-type calcium channel blockers. *Biochem. Biophys. Res. Commun.* **206**, 449–454
- 52 Kim, J. I., Takahashi, M., Martin-Moutot, N., Seagar, M. J., Ohtake, A. and Sato, K. (1995) Tyr $^{13}$  is essential for the binding of  $\omega$ -conotoxin MVIIIC to the P/Q-type calcium channel. *Biochem. Biophys. Res. Commun.* **214**, 305–309
- 53 Sato, K., Raymond, C., Martin-Moutot, N., Sasaki, T., Ohtake, A., Minami, K., Van Renterghem, C., Kim, J. I., Takahashi, M. and Seagar, M. J. (2000) Binding of Ala-scanning analogs of  $\omega$ -conotoxin MVIIIC to N- and P/Q-type calcium channels. *FEBS Lett.* **469**, 147–150
- 54 Samsó, M., Trujillo, R., Gurrola, G. B., Valdivia, H. H. and Wagenknecht, T. (1999) Three-dimensional location of the imperatoxin A binding site on the ryanodine receptor. *J. Cell Biol.* **146**, 493–499
- 55 Serysheva, I. I., Ludtke, S. J., Baker, M. R., Chiu, W. and Hamilton, S. L. (2002) Structure of the voltage-gated L-type  $\text{Ca}^{2+}$  channel by electron cryomicroscopy. *Proc. Natl. Acad. Sci. U.S.A.* **99**, 10370–10375
- 56 Brooks, B. R., Bruccoleri, R. E., Olafson, B. D., States, D. J., Swaminathan, S. and Karplus, M. (1983) CHARMM: a program for macromolecular energy, minimization, and dynamics calculations. *J. Comput. Chem.* **4**, 187–217

Received 7 August 2003/29 September 2003; accepted 9 October 2003

Published as BJ Immediate Publication 9 October 2003, DOI 10.1042/BJ20031192